



## OPEN ACCESS

## EDITED BY

Xinzhong Li,  
Henan University of Science and Technology,  
China

## REVIEWED BY

Anwar Hussain,  
COMSATS University, Pakistan  
Jiwei Zhang,  
Northwestern Polytechnical University, China  
Liyong Ren,  
Shaanxi Normal University, China

## \*CORRESPONDENCE

Chao Zuo,  
✉ zuochao@njjust.edu.cn  
Peng Gao,  
✉ peng.gao@xidian.edu.cn

RECEIVED 24 August 2024

ACCEPTED 10 September 2024

PUBLISHED 27 September 2024

## CITATION

Zheng J, Guo X, Ma Y, Wen K, An S, Wang X,  
Gao P, Qian J, Zuo C and Gao P (2024)  
Structured illumination lensless digital  
holographic microscopy (SI-LDHM).  
*Front. Phys.* 12:1485687.  
doi: 10.3389/fphy.2024.1485687

## COPYRIGHT

© 2024 Zheng, Guo, Ma, Wen, An, Wang, Gao,  
Qian, Zuo and Gao. This is an open-access  
article distributed under the terms of the  
[Creative Commons Attribution License \(CC BY\)](https://creativecommons.org/licenses/by/4.0/).  
The use, distribution or reproduction in other  
forums is permitted, provided the original  
author(s) and the copyright owner(s) are  
credited and that the original publication in this  
journal is cited, in accordance with accepted  
academic practice. No use, distribution or  
reproduction is permitted which does not  
comply with these terms.

# Structured illumination lensless digital holographic microscopy (SI-LDHM)

Juanjuan Zheng<sup>1,2,3</sup>, Xuhong Guo<sup>1,2,3</sup>, Ying Ma<sup>1,2,3</sup>, Kai Wen<sup>1,2,3</sup>,  
Sha An<sup>1,2,3</sup>, Xiaofang Wang<sup>1,2,3</sup>, Peng Gao<sup>1,2,3</sup>, Jiaming Qian<sup>4</sup>,  
Chao Zuo<sup>4\*</sup> and Peng Gao<sup>1\*</sup>

<sup>1</sup>School of Physics, Xidian University, Xi'an, China, <sup>2</sup>Engineering Research Center of Information Nanomaterials, Universities of Shaanxi Province, Xi'an, China, <sup>3</sup>Xi'an Engineering Research Center of Super-Resolution Optical Microscopy, Xi'an, China, <sup>4</sup>School of Electronic and Optical Engineering, Nanjing University of Science and Technology, Nanjing, China

In this work, we propose a structured-illumination lensless digital holographic microscopy (SI-LDHM). SI-LDHM illuminates a sample with 24 structured illuminations (8 orientations × 3 phase shifts) and records the defocused interferogram formed by two copies of object waves along the  $\pm 1$ st diffraction orders of each SI. The reconstructed object waves under different illumination orientations are respectively propagated to the sample plane along the +1st diffraction order and then averaged, thus yielding a clean image without the artifact of twin images. Experimental results demonstrated that thanks to the multi-oriented SI strategy, the twin image in SI-LDHM is sevenfold reduced compared to conventional DHM, while the spatial resolution is 1.15 times higher.

## KEYWORDS

quantitative phase microscopy (QPM), lensless digital holographic microscopy (LDHM), structured illumination, spatial light modulator, resolution enhancement

## 1 Introduction

Digital holographic microscopy (DHM), which combines interferometry with optical microscopy and utilizes a digital camera to record the generated hologram, has been acting as one of the most accurate quantitative phase microscopy techniques [1–3]. Different with conventional optical microscopy that renders the contrast of samples utilizing the absorption/reflection of light by the sample or fluorescence excitation/emission regime, DHM is capable of recovering intrinsic contrast for transparent or translucent samples by exploring the phase of the imaging light field. Meanwhile, DHM features another merit, i.e., autofocusing, with which an in-focused image can be obtained by digitally propagating an object wave from the hologram plane to the image plane [4]. So far, DHM has been widely applied to various fields, including industrial inspection [5, 6], biomedical study [7–11], and so on.

Often DHM employs independent object and reference waves that are separate in space, and hence it is susceptible to environmental disturbances. To alleviate this dilemma, researchers resort to vibration isolation [12], degenerative feedback [13], or common-path configurations [14–18]. Among common-path DHM configurations, point-diffraction DHM [15–17] utilizes a grating to split an object wave under investigation into two copies, one of which is filtered with a pinhole into a plane wave acting as the reference wave, and the other is retained as the object wave. This technique preserves the concept of DHM (coding the phase into interference patterns) and its simple reconstruction regime. Yet, the

contrast and consequently the signal-to-noise ratio (SNR), is sample-dependent since the reference wave is generated by pinhole fielding of the object wave spectrum. As a remedy, a polarization-grating-based point-diffraction DHM (PG-DPM) utilizing a polarization diffraction grating for beam splitting was proposed, where the fringe contrast can be adjusted by manipulating the polarization of the illumination light [18]. To further upgrade, structured illumination was incorporated into point-diffraction DHM for both resolution enhancement [4] and 3D RI imaging [19, 20].

Another important issue in DHM is spatial bandwidth product (SBP). Often, DHM employs a microscopic lens to magnify the image of a sample. Yet, it often posts a limit on the imaging SBP, for instance, a  $20\times/0.4$  objective usually provides a spatial resolution  $\delta = 0.61 \lambda/\text{NA} = 965 \text{ nm}$  within a field of view (FOV) of  $1 \times 1 \text{ mm}^2$ , yielding a valid SBP of 1.07 M pixels. Such SBP is around 1/10 sampling power of the state-of-the-art cameras. For example, an sCMOS camera [Basler boA6500-36cm, Basler Vision Technology (Beijing) Co., Ltd., China] has  $6560 \times 4948$  pixels (32.5 M), which is tenfold higher than lens-based DHM. Recently, Samsung electronics company recently developed a CMOS image sensor with 200 M pixels and a pixel size of  $0.56 \mu\text{m}$  [21]. To realize large-field DHM imaging, lens-based DHM resorts to mechanical translating a sample multiple times, capturing interferograms for each objective-FOV-covered region on the specimen, and digitally stitching the reconstructed image together. To alleviate this laborious process, on-chip quantitative phase microscopy approaches based on illumination scanning [22], wavelength scanning [23], and relative displacement between the sample and the image sensor [24, 25] were reported to achieve quantitative phase imaging with ultra-large spatial bandwidth product (SBP) and pixel super-resolution.

Inspired by on-chip DHM, in this work, we present and demonstrate a structured illumination lensless digital holographic microscopy (abbreviated as SI-LDHM). SI-LDHM utilizes structured illumination (SI) to generate the interference of two copies of the object waves along the  $\pm 1$ st diffraction orders of SIs, and suppresses the twin image by averaging the reconstructed object waves along different SIs. Compared to conventional LDHM, SI-LDHM is immune to environmental disturbances, and has a reduced speckle noise level and enhanced spatial resolution, benefiting from the SIs.

## 2 Methods

### 2.1 Experimental setup of SI-LDHM

The schematic diagram of the SI-LDHM system is shown in Figure 1. A 633-nm He-Ne laser is used as the illumination source. The laser output is expanded by a telescope system  $L_1$ - $L_2$ , and guided to a phase-type spatial light modulator (SLM,  $1920 \times 1080$  pixels, pixel size  $7.56 \mu\text{m}$ , DLP F6500, UPO Labs Co., Ltd., China) after passing through a cube beam splitter BS. A linear polarizer  $P$  with its transmission polarization orientation along the horizontal direction is located before the BS to optimize the modulation efficiency of the SLM. Eight groups of binary fringe patterns (featuring a period of six pixels and binary phases  $0/\pi$ ) with a grating vector azimuth  $\theta_m =$

$m\pi/8$  are loaded to the SLM sequentially,  $m = 1, 2, \dots, 8$ . The fringe patterns are shifted three times for each orientation, yielding a phase shift of  $2\pi(n-1)/3$  with  $n = 1, 2, 3$ . Then, the patterns displayed on SLM are projected via a telescope system  $L_3$ - $L_4$  to a sample, which is located with a distance  $d = 27 \text{ mm}$  above a CMOS camera ( $4,000 \times 3,000$ , pixels size  $1.85 \mu\text{m}$ , DMK 33UX226, The Imaging Source Asia Co., Ltd., China). In SI-LDHM, it is preferable to use a  $d$  within a range of tens of millimeters to guarantee a millimeter-scale separation between the  $\pm 1$  orders of SIs on the camera plane. In the middle focal plane of the telescope system  $L_3$ - $L_4$ , the spectrum of the illumination wave is filtered by a mask having two circular holes, allowing to pass only the  $\pm 1$ st diffraction orders. Therefore, sinusoidal structured illumination is generated on the sample plane. Under such an illumination strategy, two copies of the sample transmittance waves, which have a lateral shift of  $2d\sin\theta_{\text{illum}}$ , interfere with each other on the CMOS camera. Here,  $\theta_{\text{illum}}$  denotes the angle of the  $\pm 1$ st diffraction orders of the grating. After  $8 \times 3$  intensity patterns are recorded in sequence, both the amplitude and phase images of a sample can be reconstructed using the approach depicted in Section 2.2. In SI-LDHM, the maximal frame rates of the SLM and the CMOS camera are 60 frames per second (FPS) and 30 FPS. Considering SI-LDHM requests 24 interferogram recordings for one reconstruction, the imaging speed of SI-LDHM is 1.25 FPS.

### 2.2 Numerical reconstruction of SI-LDHM

In this section, we briefly elaborate the reconstruction algorithm of SI-LDHM. The structured illumination on the sample plane can be written as Equation 1:

$$A_{\text{illum}}^{m,n} = A_0 \left\{ \exp(i\vec{k}_m \cdot \vec{r} + i\phi_n/2) + \exp(-i\vec{k}_m \cdot \vec{r} + i\phi_n/2) \right\} \quad (1)$$

where  $A_0$  denotes the amplitude magnitude of the structured illumination.  $\vec{r} = x\vec{i} + y\vec{j}$  denotes the position vector;  $x$  and  $y$  are the spatial coordinates in the sample plane.  $\vec{k}_m$  is the grating vector of the  $m$ th structured illumination with  $|\vec{k}_m| = 2\pi\sin\theta_{\text{illum}}/\Lambda$ , where  $\sin(\theta_{\text{illum}}) = \lambda/\Lambda$  indicates the polar angle and  $\theta_m = (m-1)\pi/8$  the azimuth angle with  $\Lambda$  is the phase grating period and  $m = 1, 2, \dots, 8$ . Actually,  $\phi_n = 2(n-1)\pi/3$  is the phase shift of the phase grating, with  $n = 1, 2, 3$ . When a specimen is illuminated with  $A_{\text{illum}}^{m,n}$ , two object waves  $O_{m,-1}$  and  $O_{m,+1}$  are generated and propagate along the  $\pm 1$ st diffraction orders of the SI. The CMOS camera records the interferogram between the two waves, of which the intensity distribution can be written as Equation 2:

$$I_{m,n} = |O_{m,-1} + O_{m,+1} \exp(i\phi_n)|^2 \quad (2)$$

Actually, the interferogram  $I_{m,n}$  is an off-axis interferogram, and the carrier frequency  $1/14.8 \mu\text{m}^{-1}$  is induced by the angle (that is  $2.45^\circ$ ) between the  $\pm 1$ st diffraction orders of the SI. Using the reconstruction algorithm of three-step phase shifting interferometry (PSI), the complex amplitude of the real image  $O_{m,1}O_{m,-1}^*$  of the  $I_{m,n}$  can be obtained with Equation 3:

$$O_{m,1}O_{m,-1}^* = \frac{(I_{m,1} - I_{m,2}) \cdot [1 - \exp(-i2\pi/3)] - (I_{m,1} - I_{m,3}) \cdot [1 - \exp(i2\pi/3)]}{5.196i} \quad (3)$$

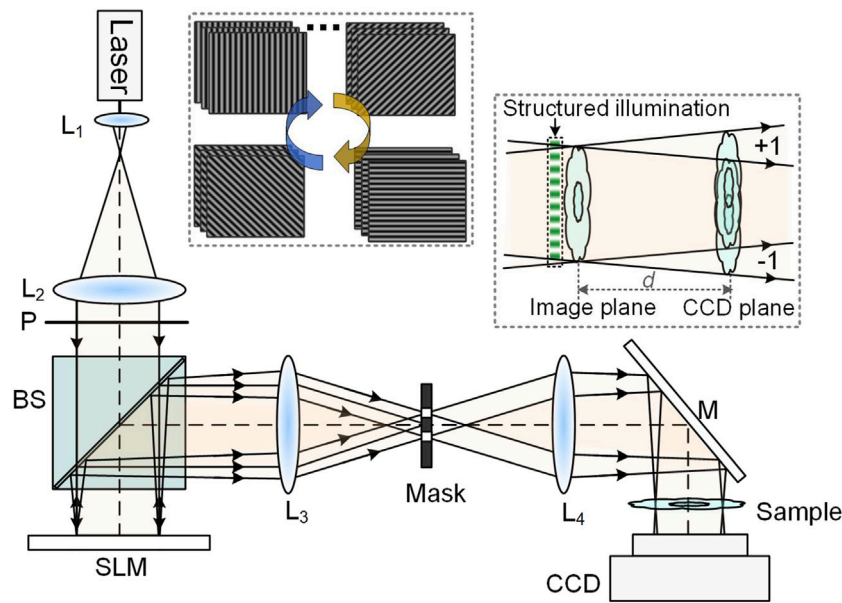


**FIGURE 1** Schematic diagram of SI-LDHM. BS, beamsplitter; CCD, charge-coupled device;  $L_1$ - $L_4$ , achromatic lens; M, Mirror; P, polarizer; SLM, spatial light modulator. The upper-left inset shows four phase gratings loaded to SLM sequentially, and the lower-right inset shows the schematics of interferogram forming with structured illumination.

As shown in Figure 3A,  $O_{m,1}O_{m,-1}^*$  contains two copies of object waves  $O_{m,1}$  and  $O_{m,-1}^*$ , which have the opposite defocusing distances  $+d$  and  $-d$ , respectively. Digital refocusing of  $O_{m,1}$  is performed by propagating  $O_{m,1}O_{m,-1}^*$  for a distance of  $d$ , using Equation 4:

$$O_{m,1}^{foc} O_{m,-1}^{defoc*} = IFT \left\{ FT \left\{ O_{m,1} O_{m,-1}^* \cdot \exp \left( -i \vec{k}_m \cdot \vec{r} / 2 \right) \right\} \cdot \tilde{W}(\xi, \eta) \cdot \exp \left[ i k d \sqrt{1 - (\lambda \xi)^2 - (\lambda \eta)^2} \right] \right\} \quad (4)$$

where  $FT[\cdot]$  and  $IFT[\cdot]$  represent the Fourier transform and inverse Fourier transform operators, respectively. The term  $\exp(-i \vec{k}_m \cdot \vec{r} / 2)$  enforces the propagation along the reverse direction of the  $+1$ st diffraction order of the SI. The refocusing yields the amplitude and phase distribution of the refocused  $O_{m,1}O_{m,-1}^*$ , namely,  $O_{m,1}^{foc} O_{m,-1}^{defoc*}$ . In  $O_{m,1}^{foc} O_{m,-1}^{defoc*}$ , the image of  $O_{m,1}^{foc}$  becomes focused and, is shifted back to its original position on the CMOS camera (shown with the black-dash circle in Figure 3A). By contrast, while the image of  $O_{m,-1}^{defoc*}$  becomes further defocused by  $2d$ , and is laterally translated for a distance of  $2d \cdot \tan \theta_{illum}$  from the image of  $O_{m,1}^{foc}$ . Therefore, a clean image of  $O_{m,1}^{foc}$  can be obtained by averaging  $O_{m,1}^{foc} O_{m,-1}^{defoc*}$  under eight groups of SIs.

$$O_{ave} = \frac{1}{M} \cdot \sum_{m=1}^M O_{m,1}^{foc} O_{m,-1}^{defoc*} \quad (5)$$

After the averaging operation in Equation 5, the contrast of the twine image is reduced by a factor of eight. We also find that the defocusing of  $2d$  acts as another key factor in reducing the contrast of the twine image  $O_{m,-1}^*$ . Meanwhile, the spatial resolution of the reconstructed  $O_{ave}$  is enhanced since the  $\pm 1$ st diffraction orders of the SIs shift the object wave spectrum in a way that some high-frequency components of the object wave beyond the NA of the system are downshifted and are finally recorded in the interference

patterns. The final spatial resolution is determined by  $\lambda z / (L + 2d \cdot \tan \theta_{illum})$ , where  $\theta_{illum}$  is the oblique angle (the polar angle with respect to the propagation direction) of the  $\pm 1$ st diffraction orders of the SIs,  $L$  is the lateral size of the CMOS camera,  $2d \cdot \tan \theta_{illum}$  is the expansion of the hologram on each lateral direction. It is worth mentioning that, in this work, three-step phase shifting is used for each orientation of the phase grating in order to achieve higher spatial resolution. Alternatively, off-axis DHM reconstruction regime can be used to reconstruct  $O_{m,1}O_{m,-1}^*$  from a single SI-generated interferogram. In this case, the amplitude and phase images can be reconstructed using only eight structured illuminations (skipping the phase shifting operation). The pros and cons of these two schemes lie in the following: The phase-shifting scheme (as adopted in this study) can achieve the highest spatial resolution twice the pixel size of the image sensor [26]. By contrast, the latter one (off-axis DHM reconstruction) can only achieve the highest spatial resolution that is four-fold the pixel size of the image sensor due to the necessity of spectrum separation of different frequency terms during the spectrum selection [27].

### 3 Experimental results

A micro-ruler surrounded by a ring etched on a glass plate was used as the sample to test the feasibility of SI-LDHM. 8 (orientation)  $\times$  3 (phase-shifting) fringe patterns with a period of six pixels were loaded sequentially to the SLM, and the CMOS camera recorded interferograms when the sample is illuminated by each SIs. Figures 2A–C show the interferograms recorded under the SIs of 8 orientations (along the Y direction) and 3 phase shifts (along the X direction). It can be seen that under each SI, there are two copies of object images, which are rotated with the SI orientation.

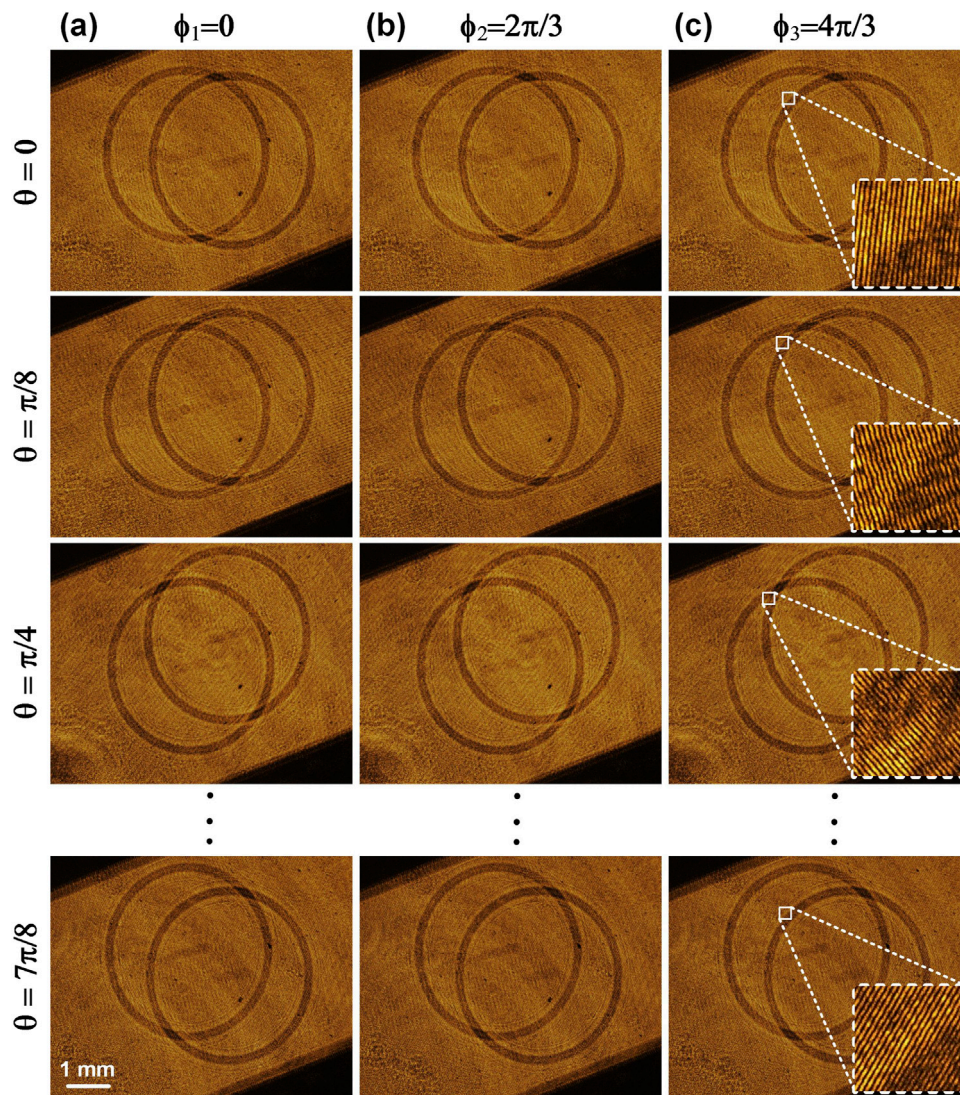


FIGURE 2

The interferograms generated by loading different phase gratings onto the SLM. (A–C) The phase-shifted interferograms generated by SIs with different phase shifts (along the X direction) and different orientations (along the Y direction). The insets in (C) show the magnified view of a rectangular area.

The inset in Figure 2C shows the fringe patterns in the interferogram, featuring a period of  $22.6 \mu\text{m}$ , sampled by 12 pixels. The complex amplitude of  $O_{m,1}O_{m,-1}^*$  was reconstructed using Equation 3, and Figure 3A illustrates the reconstructed amplitude image of the sample. The defocus distances of the images  $O_{m,1}$  and  $O_{m,-1}^*$  from the sample plane are 27 mm and  $-27$  mm, respectively, resulting in similar intensity distributions. Once  $O_{m,1}O_{m,-1}^*$  was digitally propagated for a defocusing distance of  $-27$  mm to the sample plane along the +1st diffraction order of the SI using Equation 4, the real image of  $O_{m,1}$  became focused, while the twin image  $O_{m,-1}^*$  became increasingly defocused by 54 mm, shown in Figure 3B. After the 8 refocused images of  $O_{m,1}O_{m,-1}^*$  along different SIs were averaged, the obtained amplitude of the sample is shown in Figure 3C. It can be seen that both the micro-rule and the ring have sharp structures, and the artifacts of twin images are well suppressed. The contrast of

the twin image was evaluated quantitatively by analyzing the intensity modulations along the short lines in (b) and (c) with  $V=(I_{\text{max}} - I_{\text{min}})/(I_{\text{max}} + I_{\text{min}})$ . Here,  $I_{\text{max}}$  and  $I_{\text{min}}$  are the maximal and minimal intensity of the line. The analysis turns out that  $V = 0.43$  for a single structured illumination and  $V = 0.06$  after averaging the reconstructions under eight groups of structured illuminations, implying a sevenfold reduction of the twin image contrast. Despite eight groups of SIs being demonstrated in this study, fewer illumination numbers can be used to enhance the imaging speed of SI-LDHM. While four illumination orientations are the minimum for SI-DHM to guarantee that the contrast of the twin image is lower than 25% of the signal.

In SI-LDHM, the lateral dimensions of the rectangular hologram are 7.5 and 5.6 mm, respectively. The size of the hologram limits the spatial resolution of conventional LDHM imaging mode to  $\delta = \lambda z/L = 3.0 \mu\text{m}$ . The SI enhances effective hologram size by  $2d \cdot \tan\theta_{\text{illum}}$

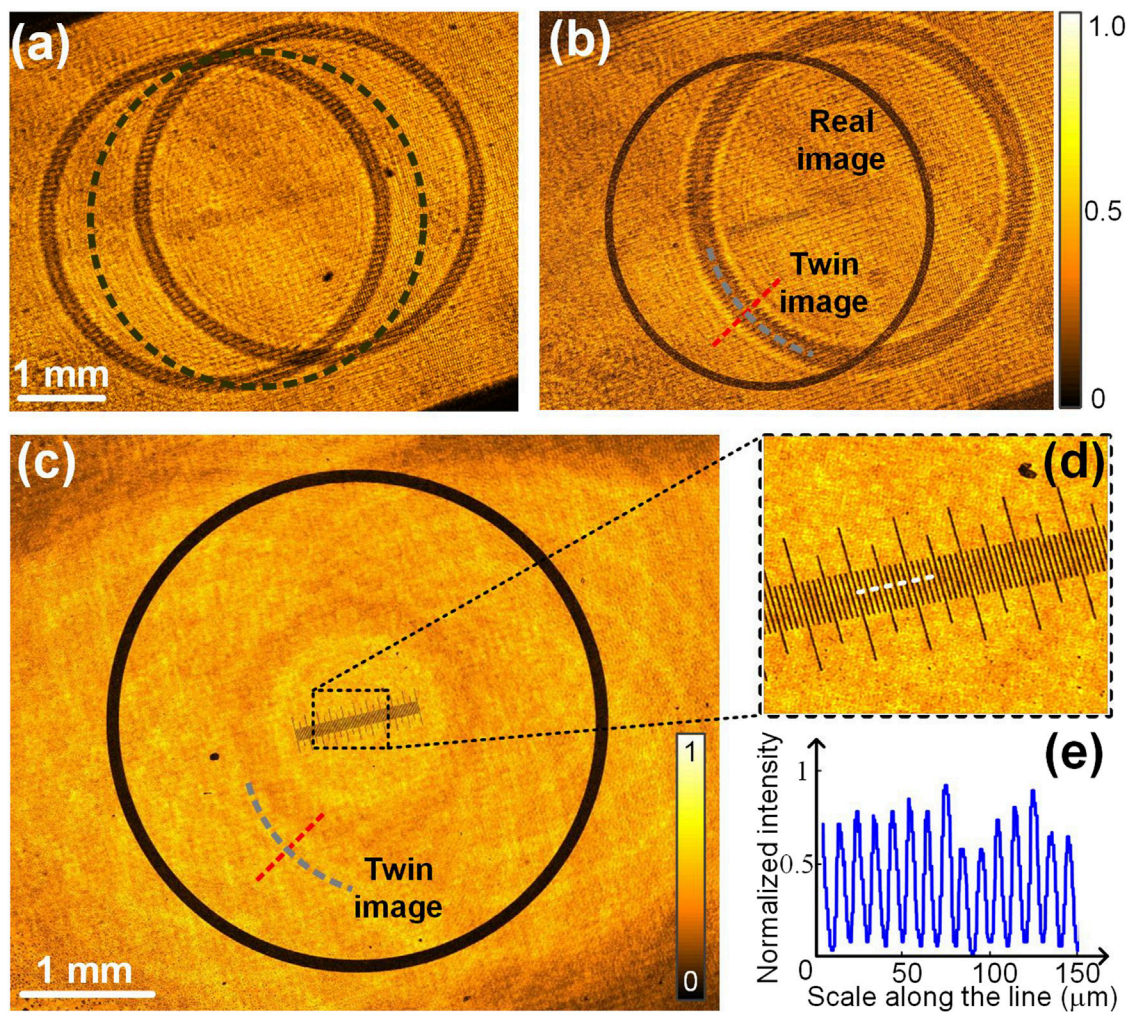


**FIGURE 3** Reconstruction of SI-LDHM. The amplitude image of  $O_{m,1}O_{m,-1}^*$  before propagated to the image plane (A) and after propagated to the image plane (B) along the +1 diffraction order of the structured illumination. The black-dash circle in (A) shows the original position of the sample upon being illuminated with an on-axis plane wave. (C) The reconstructed amplitude image after the averaging operation in Equation 5. (D) The magnified close-up in (C). (E) The intensity distribution along the dash-white line in (D).

for two orthogonal directions and consequently enhances the lateral resolution to  $\delta = \lambda z / (L + 2d \cdot \tan \theta_{\text{illum}}) = 2.6 \mu\text{m}$ . It can be seen from Figure 3D that the tiny ticks with a period of  $10 \mu\text{m}$  are well resolved. The high-pitch width of the black line is  $4 \mu\text{m}$ , as is shown in Figure 3E. The spatial bandwidth product (SBP) of SI-LDHM is  $7.5 \times 5.6 \times 10^6 / 2.6^2 = 6.2 \times 10^6$ , which is sixfold higher than that of lens-based DHM equipped with a  $20\times/0.4$  objective [the valid SBP:  $1 \times 1 \times 10^6 / (0.61\lambda/\text{NA})^2 = 1.07 \times 10^6$ ].

Eventually, SI-LDHM was applied to inspect waveguides fabricated in a silica glass plate. With a single line scan of a focused femtosecond laser over a crystal bulk, the structures with channel geometry were produced [28]. Refractive index (RI) distribution is one of the essential parameters of waveguides. Yet, due to their transparency, conventional optical microscopy can not visualize the waveguides' structure, let alone quantitatively inspect their 3D RI distribution. By contrast, SI-LDHM manages to provide both the amplitude image and phase image of the waveguides. Compared to the amplitude image in Figure 4A, the phase image

in Figure 4B has higher contrast. Notably, it is found from the phase image that the core of the waveguide has a higher RI than the cladding. Such RI distribution was induced by silica expansion from the center to the periphery of the scanned line due to the heating effect. The average power, repetition rate, and scanning speed of the femtosecond laser should be controlled delicately; otherwise, it will lead to the failure of waveguide fabrication (the two black-dotted lines in Figure 4A are failed waveguides due to over-burning of the laser). The above investigation implies that SI-LDHM provides a versatile way for high-throughput waveguide inspection.

## 4 Discussion

In summary, a structured-illumination lensless digital holographic microscopy (SI-LDHM) for high-throughput QPM imaging is presented. SI-LDHM utilizes a spatial light modulator (SLM) to generate 24 groups of fringe patterns (8 orientations  $\times$

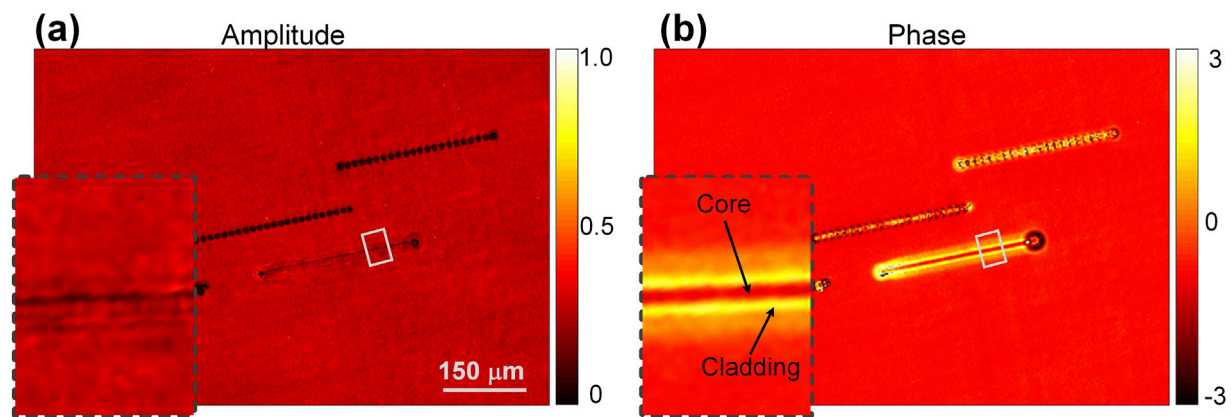


**FIGURE 4**  
SI-LDHM imaging of laser-fabricated waveguide in a glass plate. **(A)** Reconstructed amplitude image. **(B)** Reconstructed phase image. The insets in **(A)** and **(B)** show a magnified subregion of the waveguide, indicated by the white boxes.

3 phase shifts) for illumination and records the self-interference patterns of the object wave under different SIs. Utilizing the feature that the real and twin images have an opposite defocusing distance, a clean image reconstruction is obtained by refocusing each object wave along the +1st diffraction order of the SI and averaging them for all the orientations of SIs. In this study, SI-LDHM with eight groups of SIs was demonstrated for DHM imaging of a micro-ruler. Eight independent SI yield a reduction of speckle noise by a factor of 2.8 (i.e.,  $\sqrt{8}$ ) and a sevenfold reduction of the twin-image contrast. Furthermore, structured illumination with an oblique illumination angle  $\theta_{\text{illum}} = 1.8^\circ$  enhances the lateral resolution of LDHM from 3.0  $\mu\text{m}$  to 2.6  $\mu\text{m}$ .

In the future, iterative projection methods [29] and unified compressive phase retrieval frameworks with both physical constraints and sparsity priors [30] can be further used for reconstruction of SI-LDHM with sub-pixel resolution. Furthermore, 3D refractive index map can be achieved by incorporating the optical diffraction tomography (ODT) reconstruction concept [31] into SI-LDHM.

## Data availability statement

The original contributions presented in the study are included in the article/supplementary material, further inquiries can be directed to the corresponding authors.

## Author contributions

JZ: Data curation, Formal Analysis, Investigation, Writing—original draft. XG: Data curation, Writing—original draft. YM: Data curation, Writing—review and editing. KW: Data curation, Writing—review and editing. SA: Formal Analysis, Writing—review and editing. Validation. XW: Validation, Writing—review and editing. PG (7th author): Validation, Writing—review and editing. JQ: Validation, Writing—review and editing. CZ: Funding

acquisition, Validation, Writing—original draft. PG (10th author): Funding acquisition, Investigation, Methodology, Supervision, Writing—original draft.

## Funding

The authors declare financial support was received for the research, authorship, and/or publication of this article. This work was supported by National Natural Science Foundation of China (62075177, 62105251); the Key Research and Development Program of Shaanxi (2024GH-ZDXM-05); National Key Research and Development Program of China (2021YFF0700303); the Natural Science Basic Research Program of Shaanxi (Program Nos 2023-JC-YB-518, 2022JQ-122, 2023-JC-QN-0731). The Fundamental Research Funds for the Central Universities (QTZX23024, QTZX23013, XJS222803, QTZX23008, ZYTS24093 and XJSJ23137).

## Conflict of interest

The authors declare that the research was conducted in the absence of any commercial or financial relationships that could be construed as a potential conflict of interest.

The authors declared that they were an editorial board member of Frontiers, at the time of submission. This had no impact on the peer review process and the final decision.

## Publisher's note

All claims expressed in this article are solely those of the authors and do not necessarily represent those of their affiliated organizations, or those of the publisher, the editors and the reviewers. Any product that may be evaluated in this article, or claim that may be made by its manufacturer, is not guaranteed or endorsed by the publisher.

## References

- Kim MK. Principles and techniques of digital holographic microscopy. *SPIE Rev* (2010) 1:018005. doi:10.1117/6.0000006
- Mann CJ, Yu L, Lo CM, Kim MK. High-resolution quantitative phase-contrast microscopy by digital holography. *Opt Express* (2005) 13:8693–8. doi:10.1364/opex.13.008693
- Gao P, Yuan C. Resolution enhancement of digital holographic microscopy via synthetic aperture: a review. *Light: Adv Manuf* (2022) 3:105. doi:10.37188/lam.2022.006
- Gao P, Pedrini G, Osten W. Structured illumination for resolution enhancement and autofocusing in digital holographic microscopy. *Opt Lett* (2013) 38:1328–30. doi:10.1364/ol.38.001328
- Emery Y, Cuche E, Marquet F, Aspert N, Marquet P, Kuhn J, et al. Digital holography microscopy (DHM): fast and robust systems for industrial inspection with interferometer resolution. *Proc Spie-int Soc Opt Eng* (2005) 5856:930–7. doi:10.1117/12.612670
- Kebbel V, Hartmann HJ, Jüptner WP. Application of digital holographic microscopy for inspection of micro-optical components, optical measurement systems for industrial inspection II: application in industrial design. *Proc SPIE* (2001) 4398:189–98. doi:10.1117/12.445551
- Yamaguchi I, Kato J, Ohta S, Mizuno J. Image formation in phase-shifting digital holography and applications to microscopy. *Appl Opt* (2001) 40:6177–86. doi:10.1364/ao.40.006177
- Emery Y, Cuche E, Colomb T, Depeursing C, Rappaz B, Marquet P, et al. DHM (digital holography microscope) for imaging cells. *J Phys Conf Ser* (2007) 61:1317–21. doi:10.1088/1742-6596/61/1/260
- Marquet P, Rappaz B, Magistretti PJ, Cuche E, Emery Y, Colomb T, et al. Digital holographic microscopy: a noninvasive contrast imaging technique allowing quantitative visualization of living cells with subwavelength axial accuracy. *Opt Lett* (2005) 30:468–70. doi:10.1364/ol.30.000468
- Carl D, Kemper B, Wernicke G, Bally G. Parameter-optimized digital holographic microscope for high-resolution living-cell analysis. *Appl Opt* (2004) 43:6536–44. doi:10.1364/ao.43.006536
- Dubois F, Yourassowsky C, Monnom O, Legros JC, Debeir O, Ham PV, et al. Digital holographic microscopy for the three-dimensional dynamic analysis of *in vitro* cancer cell migration. *J Biomed Opt* (2006) 11:054032. doi:10.1117/1.2357174
- Toy MF, Richard S, Kühn J, Franco-Obregón A, Egli M, Depeursing C. Enhanced robustness digital holographic microscopy for demanding environment of space biology. *Biomed Opt Express* (2012) 3:313–26. doi:10.1364/boe.3.000313
- Popescu G, Ikeda T, Goda K, Best-Popescu CA, Laposata M, Manley S, et al. Optical measurement of cell membrane tension. *Phys Rev Lett* (2006) 97:218101. doi:10.1103/physrevlett.97.218101
- Zhang J, Dai S, Ma C, Xi T, Di J, Zhao J. A review of common-path off-axis digital holography: towards high stable optical instrument manufacturing. *Light: Adv Manuf* (2021) 2:1. doi:10.37188/lam.2021.023
- Medeckí H, Tejníl E, Goldberg KA, Bokor J. Phase-shifting point diffraction interferometer. *Opt Lett* (1996) 21:1526–8. doi:10.1364/ol.21.001526
- Popescu G, Ikeda T, Dasari RR, Feld MS. Diffraction phase microscopy for quantifying cell structure and dynamics. *Opt Lett* (2006) 31:775–7. doi:10.1364/ol.31.000775
- Gao P, Harder I, Nercissian V, Mantel K, Yao B. Phase-shifting point-diffraction interferometry with common-path and in-line configuration for microscopy. *Opt Lett* (2010) 35:712–4. doi:10.1364/ol.35.000712
- Zhang M, Ma Y, Wang Y, Wen K, Zheng J, Liu L, et al. Polarization grating based on diffraction phase microscopy for quantitative phase imaging of paramecia. *Opt Express* (2020) 28:29775–87. doi:10.1364/oe.404289
- Liu R, Wen K, Li J, Ma Y, Zheng J, An S, et al. Multi-harmonic structured illumination-based optical diffraction tomography. *Appl Opt* (2023) 62:9199–206. doi:10.1364/ao.508138
- Chowdhury S, Eldridge WJ, Wax A, Izatt J. Refractive index tomography with structured illumination. *Optica* (2017) 4:537–45. doi:10.1364/optica.4.000537
- Choi S, Lee S, Lee T, Ji H, Park H, Im D, et al. World smallest 200Mp CMOS Image Sensor with 0.56 $\mu$ m pixel equipped with novel Deep Trench Isolation structure for better sensitivity and higher CG (2023). Available from: <https://imagesensors.org/Past%20Workshops/2023%20Workshop/2023%20Papers/R13.pdf> (Accessed on May 22, 2023).
- Luo W, Greenbaum A, Zhang Y, Ozcan A. Synthetic aperture-based on-chip microscopy. *Light Sci Appl* (2015) 4:e261. doi:10.1038/lsa.2015.34
- Wu X, Sun J, Chen Y, Wei J, Chen Q, Poon T, et al. Wavelength-scanning pixel-super-resolved lens-free on-chip quantitative phase microscopy with a color image sensor. *Appl Photon* (2024) 9:016111. doi:10.1063/5.0175672
- Greenbaum A, Luo W, Su TW, Gorocs Z, Xue L, Isikman SO, et al. Imaging without lenses: achievements and remaining challenges of wide-field on-chip microscopy. *Nat Methods* (2012) 9:889–95. doi:10.1038/nmeth.2114
- Zhang J, Sun J, Chen Q, Li J, Zuo C. Adaptive pixel-super-resolved lensfree in-line digital holography for wide-field on-chip microscopy. *Sci Rep* (2017) 7:11777. doi:10.1038/s41598-017-11715-x
- Bhattacharya NGK. Cube beam-splitter interferometer for phase shifting interferometry. *J Opt* (2009) 38:191–8. doi:10.1007/s12596-009-0017-6
- Gao P, Yao B, Harder I, Min J, Guo R, Zheng J, et al. Parallel two-step phase-shifting digital holograph microscopy based on a grating pair. *J OPT SOC AM A* (2011) 28:434–40. doi:10.1364/josaa.28.000434
- Lv J, Cheng Y, Yuan W, Hao X, Chen F. Three-dimensional femtosecond laser fabrication of waveguide beam splitters in LiNbO<sub>3</sub> crystal. *Opt Mater Express* (2015) 5:1274–80. doi:10.1364/ome.5.001274
- Gao P, Pedrini G, Osten W. Phase retrieval with resolution enhancement by using structured illumination. *Opt Lett* (2013) 38:5204–7. doi:10.1364/ol.38.005204
- Gao Y, Cao L. Iterative projection meets sparsity regularization: towards practical single-shot quantitative phase imaging with in-line holography. *Light: Adv Manuf* (2023) 4:1–53. doi:10.37188/lam.2023.006
- Zhou N, Zhang R, Xu W, Zhu R, Tang H, Zhou X, et al. High-speed high-resolution transport of intensity diffraction tomography with Bi-plane parallel detection. *Laser Photon Rev* (2024):2400387. doi:10.1002/lpor.202400387